Dental Materials 39 (2023) 894–902

Contents lists available at ScienceDirect

Dental Materials

journal homepage: www.elsevier.com/locate/dental

Optical behavior of 3D-printed dental restorative resins: Influence of thickness and printing angle

Cristina Espinar [a], Alvaro Della Bona [b], Maria Tejada-Casado [c], Rosa Pulgar [a], María M. Pérez [c,*]

[a] Department of Stomatology, Faculty of Dentistry, Colegio Máximo, Campus de Cartuja s/n. University of Granada, 18071, Granada, Spain
[b] Post-Graduate Program in Dentistry, Dental School, University of Passo Fundo, Campus I, Passo Fundo, RS, Brazil
[c] Department of Optics, Faculty of Science, Campus Fuentenueva, Edificio Mecenas, s/n. University of Granada, 18071, Granada, Spain

ARTICLE INFO

Keywords:
3D-printed dental resin
Thickness
Printing orientation
Kubelka-Munk Theory
Scattering
Absorption
Transmission
Light reflectivity

ABSTRACT

Objectives: To evaluate the influence of thickness and printing angle on the optical properties of 3D-printed dental restorative resins.

Methods: Four 3D printing resin systems were evaluated: DFT-Detax Freeprint Temp; FP- Formlabs Permanent Crown; FP- Formlabs Temporary CB; and GCT- GC Temporary-. Samples from each material were printed at 0° and 90°, and polished up to 0.5, 1.0, 1.5 and 2.0 mm thickness. Scattering (S), absorption (K) and albedo (a) coefficients, transmittance (T%), light reflectivity (RI) and infinite optical thickness (X_∞) were calculated using Kubelka-Munk's model. Data were statistically analyzed using Kruskal–Wallis¸ Mann-Whitney tests, and VAF coefficient.

Results: The spectral distribution on S, K, T%, RI, X_∞ were wavelength dependent. Although the spectral behaviors were similar for all the specimens evaluated, the values of S, K, T% and X_∞ presented significant differences between specimen thicknesses for all the materials used and for both printing orientations. Values for S and K increased, and T% and X_∞ decreased. Significant differences between 0° and 90° were found for RI values at 0.5 and 1.0 mm thick samples, for S and K at 2.0 mm, for X_∞ at 0.5 and 1.0 mm for DFT, and at 0.5 mm for FT.

Conclusions: Optical properties of 3D-printed restorative resins vary between thicknesses, and could be affected by the building orientation. Therefore, these factors should be considered in order to improve the biomimetic potential of 3D-printed dental restorative resins.

Clinical significance: Understanding the optical behavior of the 3D-printed restorative resins is essential to optimize their clinical performance.

1. Introduction

In recent years, the clinical workflow in dental practice has been revolutionized by computer-aided design (CAD) and manufacturing (CAM) [1]. Even more recent, additive manufacturing (AM) technology, also known as 3D printing [1], is gaining rising popularity mainly due to the reduction of the material waste and the production of multiple restorations without increasing manufacturing time [2,3].

In dentistry, stereolitography (SLA) and digital light processing (DLP) are the most commonly used technologies [4]. In both printing systems, an object is built through deposition of consecutive layers of photosensitive material that is readily polymerized [2]. AM has experienced significant advances becoming an useful tool to solve clinical needs in restorative dentistry [3,5,6]. 3D printing resins have been validated for temporary and midterm use (2 years maximum), and they are appropriate for crowns, inlays, onlays and bridges [7,8].

Anisotropy and low filler content are the major flaws of AM due to the layered fabrication technique, which will have an influence on the physical properties of the printed resin-based structures [9]. Most studies on novel restorative 3D printing polymers have focused on physical and mechanical properties, dimensional accuracy and strength [3,10–13]. However, adequate knowledge on color behavior, perception and appearance of dental resins, which is obtained by learning about optical characterization, can assist clinicians to select the proper material and shade to achieve a natural appearance in dental restorations. In this context, a recent review [14] reported that color and optical

* Correspondence to: Department of Optics Faculty of Sciences, Mecenas building, Campus Fuentenueva. University of Granada, Spain.
E-mail address: mmperez@ugr.es (M.M. Pérez).

https://doi.org/10.1016/j.dental.2023.08.003
Received 17 April 2023; Received in revised form 27 July 2023; Accepted 7 August 2023
Available online 17 August 2023

properties of 3D-printed restorative polymers were not adequately evaluated and characterized in the scarce existing literature.

Various factors, such as printing parameters, layer thickness and the printer itself, affect the final material properties [15]. In particular, the building direction, meaning the layer construction orientation, is an important printing parameter that could assist in modulating the anisotropy and physical weaknesses of the printed material due to the layering fabrication technique [9]. It been proven that the printing orientation affects the mechanical properties [10–13] and the printing accuracy [16] of 3D printing restorative resins. However, the influence of printing orientation and structural thickness on the optical properties (scattering, absorption, light reflectance and transmittance) has not been evaluated.

Although light propagation in turbid media may be simulated by Monte Carlo techniques or mathematically modeled with a theory based on radiative transfer equation (RTE), these models have a high computational cost, lacking analytics, and numerical solutions without the use of approximations [17,18]. A recognized alternative in the field of optics consists in using the two-flux model, which under some specific approximations, is an angularly integrated solution of the RTE. A simpler one-dimensional model is provided by the two-flux Kubelka--Munk (K-M) reflectance theory [19,20], which is still widely used because of its relative simplicity for translucent materials, allowing calculations for scattering and absorption coefficients (S and K), and considering the reflectance over the thickness of the material, and the reflectance of the backing [21]. Thus, this model, enables the extraction of spectral absorption and scattering coefficients of a given material of known thickness using simple analytical calculation, by means of only two optical measurements: the reflectance factors of the layer in optical contact with a white background and with a black background, provided the spectral reflectance factor of the black and white backgrounds are known. The white background used in this method is generally opaque, highly reflecting and strongly scattering. These characteristics are important to meet the physical assumptions underlying the model, i.e., the fact that incident and reflected lights are perfectly diffused. This reflectance theory model has been used to evaluate the optical behavior of dental resin composites [21–26].

Therefore, the aim of this study was to apply the two-flux Kubelka-Munk model to evaluate the optical behavior of 3D-printed dental restorative resins, testing the hypotheses that (1) scattering (S), absorption (K), transmittance (T %) spectral behavior, albedo coefficient (a) and light reflectivity (RI), and infinite optical thickness (X_∞) in 3D-printed restorative resins is influenced by the material thickness, and (2) the spectral behavior of S, K, T%, RI, and X_∞ in 3D-printed restorative resins is influenced by the printing angle.

2. Materials and methods

2.1. Specimen fabrication

Polymer-based 3D printing specimens were prepared in a square shape (10 mm × 10 mm) (Fig. 1) (n = 3) using four different 3D printing resins indicated for dental restorations (Table 1). The specimens were printed using the 3D printer recommended by each material's manufacturer.

A CAD software (Autodesk Fusion 360, Autodesk Inc., San Rafael, California, USA) was applied for specimen design producing four standard tessellation language (STL) files (one per thickness), which were used to manufacture the specimens from the evaluated materials. The STL files were exported to a slicing software (Table 1), where sufficient support structures were added. Manufacturer stablished parameters for exposure time, a 50 μm layer thickness and two different printing orientations (0° and 90°) to the building platform surface (Fig. 2A), were used for printing the specimens.

The printed constructs (Fig. 2B-C) were carefully post-processed in accordance with the manufacturer's recommended instructions (Table 2). Then, the specimens were polished under water cooling on the bottom side (the closer to the printing platform) (Fig. 1) using a sequence of silicon carbide (SiC) papers of decreasing grit (500–800–1200–2000–4000). A digital caliper (Mitutoyo, Europe GmbH, Germany) was used to control specimen thickness during the polishing process to a final thickness of 0.50 mm ± 0.01 mm, 1.00 mm ± 0.01 mm, 1.50 mm ± 0.01 mm and 2.00 mm ± 0.01 mm. The specimens were classified and stored in the dark.

2.2. Spectral reflectance measurement

To measure the spectral reflectance of all samples, a non-contact measuring set up was used. The system was comprised of a xenon arc lamp (300 W, Newport Stratford Inc., Franklin, MA, USA), two fiber-optic light cables (Model 70050; Newport Stratford Inc., Franklin, MA, USA) and a spectroradiometer (PR 670- Photo Research, Chatsworth, CA, USA) positioned on a custom-made optical table. The spectroradiometer was placed at 40 cm from the samples and with the CIE 45°/0° illuminating/measuring geometry, in order to avoid specular reflection. Standard backgrounds (50 ×50 mm ceramic tiles; Ceram, Staffordshire, UK) white (L* = 94.2, a* = 1.3 and b* = 1.7) and black (L* = 3.1, a* = 0.7 and b* = 2.4) were used to place and measure the spectral reflectance of all specimens at every 2 nm in the visible range (380–780 nm). Saturated sucrose solution, with an approximately 1.5 refraction index, was placed between specimen and background, as the optical contact. For each specimen, three reflectance measurements without replacement were taken and the results were averaged.

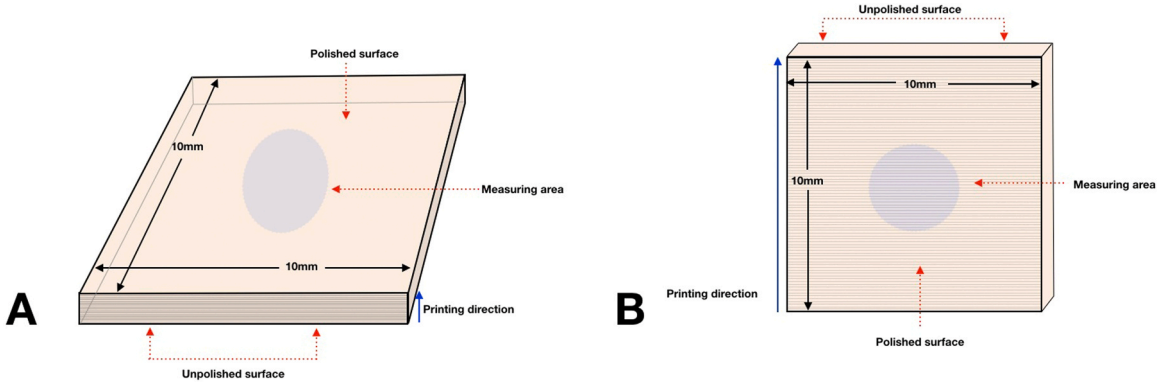

Fig. 1. Square-shaped specimen used in the study. A - Specimen size, printing orientation (0° or horizontal printing) and polished surface. B - Specimen size, printing orientation (90° or horizontal printing) and polished surface.

Table 1
Information about the 3D printing restorative resins evaluated in this study.

Brand name	Manufacturer	Material composition	Printer and software	Shade/Lot numbers
DFT- Detax Freeprint Temp	DETAX GmbH, Ettlingen, Germany	Monomers and oligomers/polymers encapped with a (meth-) acrylate group; - < 5% of modified silicic acids; - Isopropylidenediphenol peg-2 dimethacrylate (45-<60%); - 7,7,9(or 7,9,9)-trimethyl-4,13-dioxo-3,14-dioxa-5,12-diaza-hexadecane-1,16-diyl bismethacrylate (30-<35%); - 1,6-hexanediol dimethacrilate (1-<5%) - 2-hydroxyethyl methacrylate (1-<5%) - Diphenyl(2,4,6-trimethylbenzoyl)phosphine oxide (1-<5%) - Hydroxy propyl methacrylate (1-<5%) - Phenyl bis(2,4,6-trimethylbenzoyl)-phosphine oxide (<1%)	Asiga Max UV[1] Asiga Composer Software (Asiga HQ, Alexandria, NSK, Australia)	A3: 240201
FT- Formlabs Temporary CB	Formlabs Inc., Somerville, MA, USA	Ceramic micro-filler (lower content)*	3D Form 3B+[2] Preform Software (Formlabs Inc.,35 Medford, Somerville, MA 02143, USA)	A3: 600130
FP- Formlabs Permanent Crown	Formlabs Inc., Somerville, MA, USA	Ceramic micro-filler (higher content)*	3D Form 3B+[2] Preform Software (Formlabs Inc.,35 Medford, Somerville, MA 02143, USA)	A3: 600164
GCT- GC TempPrint	GC Corporation, Tokyo, Japan	- Uretane dimethacrylate (55–65%) - Dimethacrilate (15–25%) - Silicone dioxide (15–25%) - Photoiniciator (1–5%) - Pigment (trace)	Asiga Max UV[1] Asiga Composer Software (Asiga HQ, Alexandria, NSK, Australia)	Medium: 2010091

[1] Digital light processing (DLP) printer. Asiga HQ, Alexandria, NSK, Australia.
[2] Stereolithography (SLA) printer. Formlabs Inc.,35 Medford, Somerville, MA 02143, United States.
*The manufacturer did not provide detailed information.

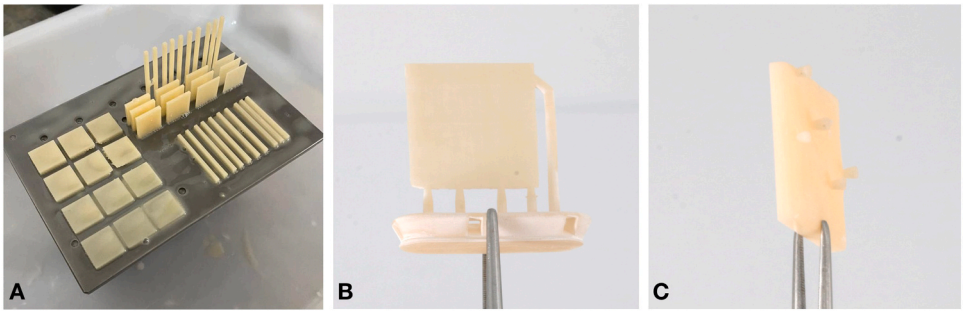

Fig. 2. A- 0° and 90° printed specimens in the building platform; B- 90° and C- 0 ° specimens printed using Formlabs 3D Form 3B+.

Table 2
Post-processing procedures for the printed samples according to the manufacturer's instructions.

Post-processing procedures	DFT	FT	FP	GCT
Specimens removal from building platform	[1] Careful removal. Using a scraper.	[2] Careful removal. Using a scraper.	[2] Careful removal. Using a scraper.	[1] Careful removal. Using a scraper.
Pre-Cleaning	[2] Sonic bath with 99,9% isopropyl alcohol for 2 min.	[1] FormWash (Formlabs Inc., Somerville, MA, USA) Fresh 99,9% Isopropyl alcohol 3 min.	[1] FormWash (Formlabs Inc., Somerville, MA, USA) Fresh 99,9% Isopropyl alcohol 3 min.	[2] Sonic bath with 99,9% isopropyl alcohol for 2 min.
Cleaning	[4] Sonic bath with fresh 99,9% isopropyl alcohol for 3 min.	[3] FormWash using fresh 99,9% isopropyl alcohol for 3 min.	[3] FormWash using fresh 99,9% isopropyl alcohol for 3 min.	[3] Sonic bath with fresh 99,9% isopropyl alcohol for 2 min.
Drying	[5] Compressed air.	[4] Compressed air.	[4] Compressed air.	[4] Compressed air.
Support structures removal	[3] Low speed rotary instrument (Marathon N3S S07, Supershu).	[6]* Low speed rotary instrument (Marathon N3S S07, Supershu).	[6]* Low speed rotary instrument (Marathon N3S S07, Supershu).	[6] Cutting pliers and a carbide bur
First post-curing	[6] Otoflash G171-N2 (NK Optik GmbH Baierbrunn, Germany) Xenon flash (2 ×2000 flashes Nitrogen) 300–700 nm light	[5] FormCure (Formlabs Inc., Somerville, MA, USA). 20 min 60 °C Heat + 405 nm light	[5] FormCure (Formlabs Inc., Somerville, MA, USA). 20 min 60 °C Heat + 405 nm light	[5] Otoflash G171-N2 (NK Optik GmbH Baierbrunn, Germany) Xenon flash (2 ×400 flashes Nitrogen) 300–700 nm light
Second post-curing	Not necessary	[7] FormCure (Formlabs Inc., Somerville, MA, USA). 20 min 60 °C	[7] FormCure (Formlabs Inc., Somerville, MA, USA). 20 min 60 °C	[7] Otoflash G171-N2 (NK Optik GmbH Baierbrunn, Germany) Xenon flash (2 ×400 flashes Nitrogen)

The sequence of the post-processing procedures for each material (per column) is indicated by superscript numbers.
*White surface residue was removed using Perlablast Micro (Bego GmbH & Co., Bremen, Germany).

2.3. Optical properties

The Kubelka-Munk scattering (S) coefficient, absorption (K) coefficient, transmittance (T %), reflectance at infinite thickness (RI) and infinite optical thickness (X_∞) were algebraically calculated as described in previous studies [21,27]. Since these optical parameters are wavelength-dependent, their values vary across the visible spectrum.

The absorption coefficient (μ_a) and the reduced scattering coefficient (μ_s') used in light transport theory can be properly obtained from S and K using an empirical non-linear relationship as follows [28]:

$$S = 0.408\mu_s'$$

$$K = \mu_a + 0.882\left(\mu_a\mu_s'\right)^{0.72}$$

where S, K, μ_a and μ_s' are expressed in units of cm^{-1}. Finally, the albedo coefficient was used to assess how absorption and scattering processes contribute to the extinction the light when passing through an analyzed 3D-printed sample:

$$a = \frac{\mu_S'}{\mu_S' + \mu_a}$$

2.4. Statistical analysis

In order to assess the spectral similarity regarding Kubelka-Munk coefficients and transmittance, the VAF (Variance Accounting For) coefficient was employed. This was done using the Cauchy-Schwarz inequality according to the following equation:

$$VAF = \frac{\left(\sum_{k=380}^{780} a_k.b_k\right)^2}{\left(\sum_{k=380}^{780} a_k^2\right)\left(\sum_{k=380}^{780} b_k^2\right)}$$

where a_k is the spectral value for T%, K coefficient and S coefficient (from 400 to 780 nm), and b_k is the corresponding for another measurement in thickness, printed angle and 3D-printed resin material. When the VAF coefficient approaches unity (100 %), it indicates that the two curves being compared are highly similar to each other.

To account for unequal variances among the parameters being evaluated in this study, Levene's test of homogeneity of variance was performed with a significant level of $\alpha = 0.05$. Kruskal–Wallis one-way analysis of variance by ranks was employed to analyze the effects of changes in thickness and between printing angles for the optical properties (S, K, T%, RI and X_∞). Pair-wise comparisons were conducted using the Mann-Whitney U test, with a Bonferroni correction applied to adjust for multiple comparisons (significance level set at $p < 0.005$). The statistical analysis was carried out using a standard statistical software package (SPSS Statistics 20.0.0, IBM Armonk, New York USA).

3. Results

Figs. 3–5 depict the spectral distribution of scattering and absorption coefficients (S and K), and transmittance (T %) as function of wavelength for the 3D-printed resins evaluated with different thicknesses and printing orientations. Considering scattering coefficient (S), the VAF analysis showed that there is good spectral behavior matches (VAF>98.5 %) between the four thicknesses and between the two printing angles for each 3D-printed dental resin evaluated (Fig. 3). The specimens showed an abrupt ramp-up increase in S values from 400 to about 450 nm, then a slight decrease of the scattering coefficient until 780 nm. The 2 mm thick GCT resin exhibited a peak at 475 nm. S showed a significant increase from 0.5 to 2.0 mm thickness ($p < 0.001$) for all 3D-printed resins evaluated. GCT samples showed the highest S values for all thicknesses and both printing angles. For each thickness, no significant differences values were found between the two printing orientations ($p > 0.05$), except for 2.0 mm thick specimens of all resins and 1.0 mm thick samples from DFT.

Considering the experimental thicknesses and both printing angles

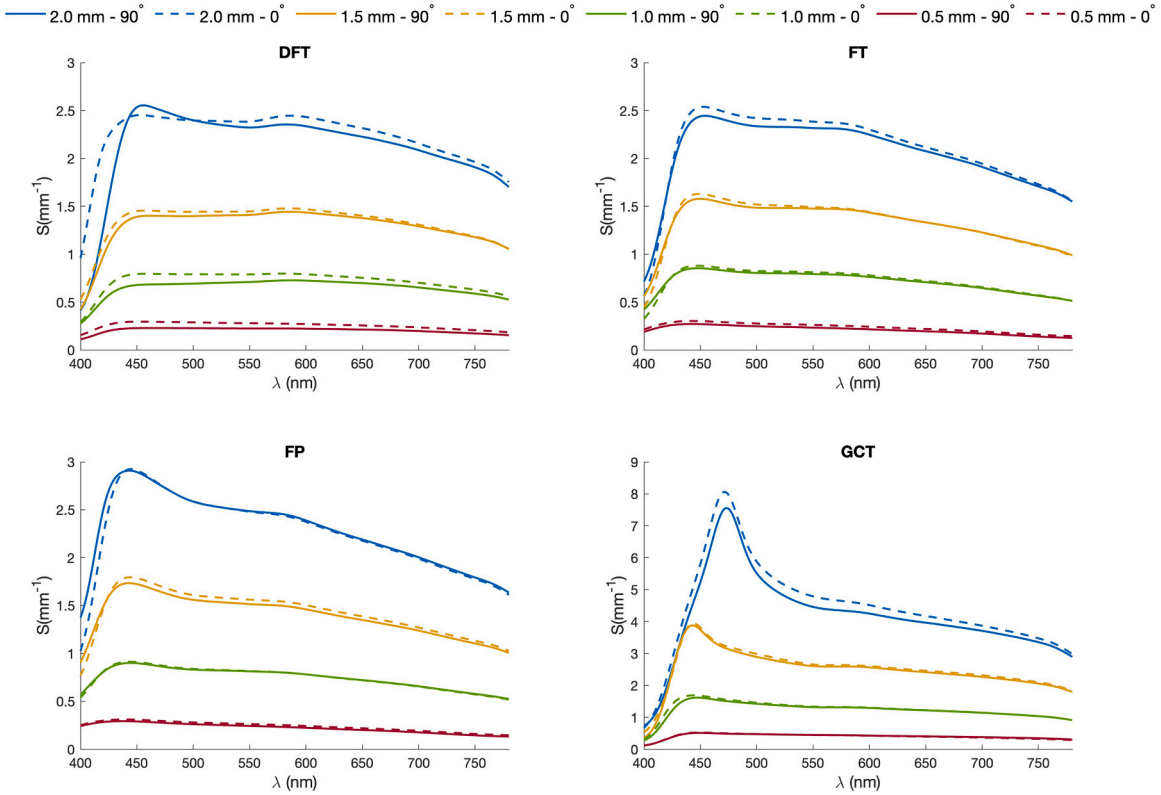

Fig. 3. Mean values of scattering coefficient (S) of all materials, thicknesses and printing orientations.

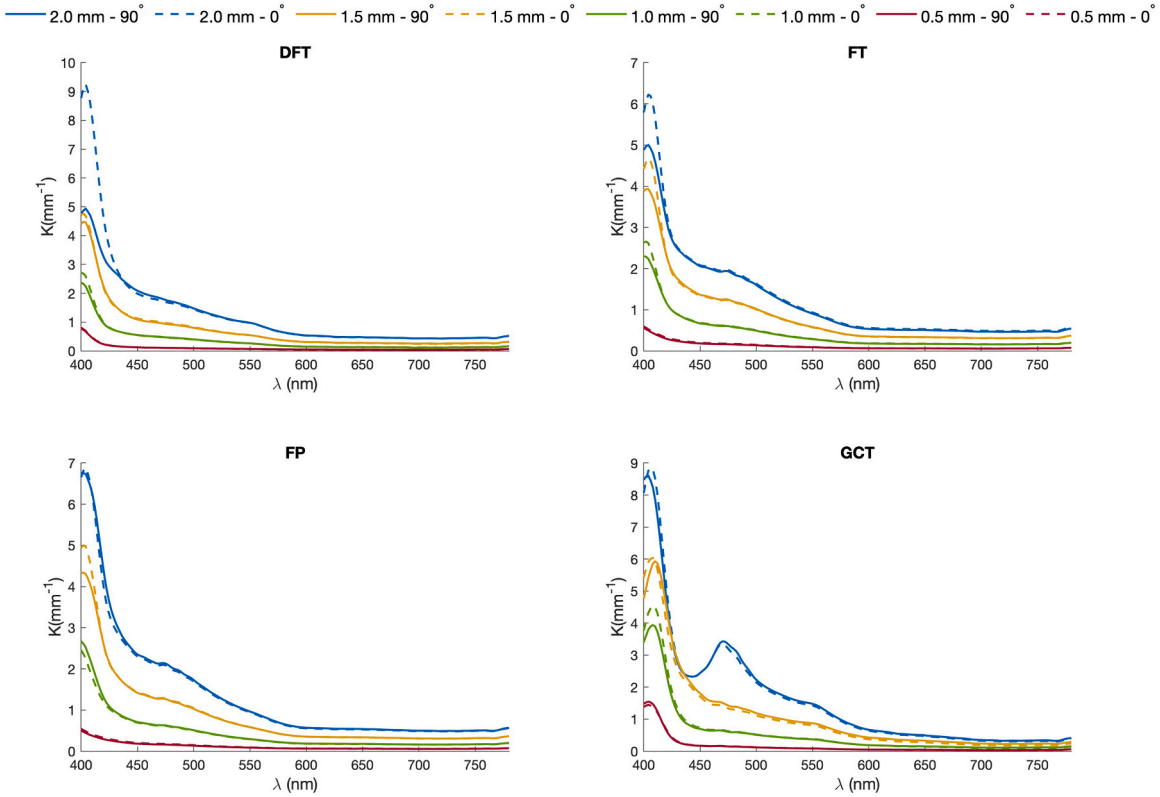

Fig. 4. Mean values of absorption coefficient (K) of all materials, thicknesses and printing orientation.

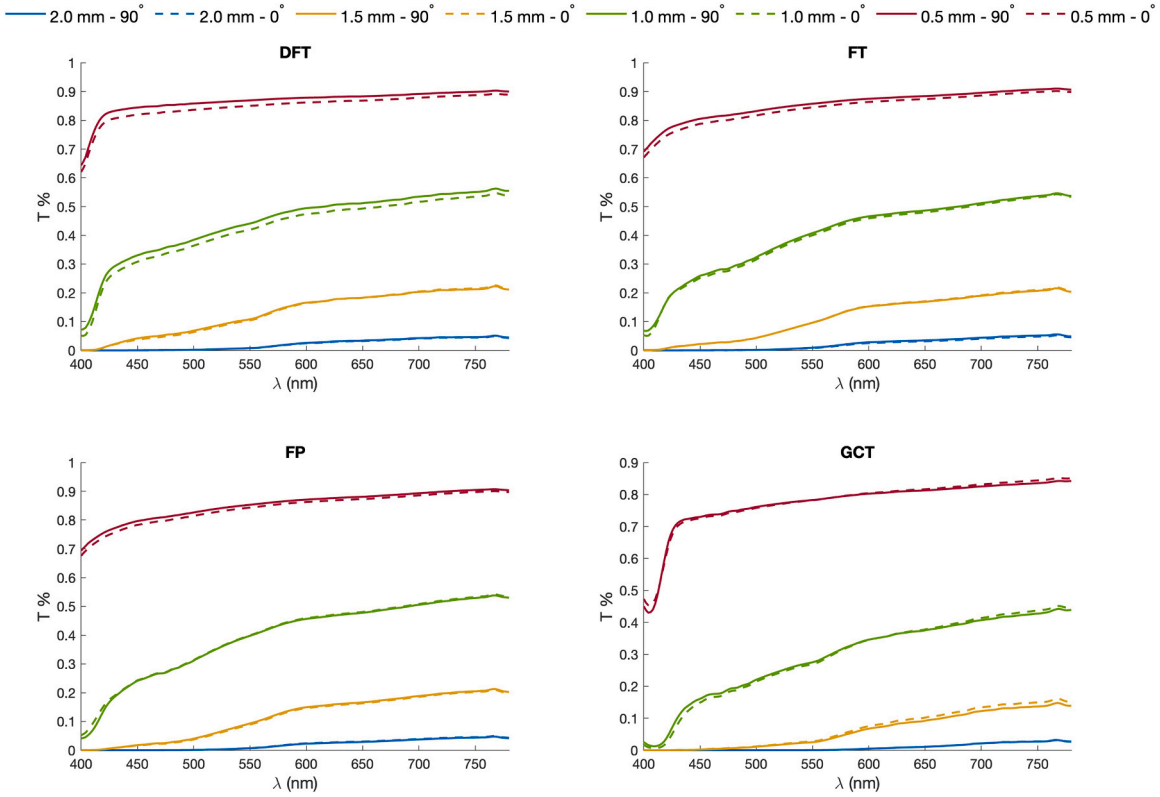

Fig. 5. Mean values of Transmittance (T%) of all materials, thicknesses and printing orientation.

used for the evaluated 3D-printed dental resins, the spectral distribution pattern of K showed a fast drop, reducing the values near zero for long wavelengths. K exhibited a significant increase from 0.5 to 2.0 mm thickness for all resins and for both printing angles ($p < 0.001$). A similar spectral behavior (VAF>98.0%) was found for K, but 0.5 mm and 2.0 mm GCT samples, that in comparison with 0.5 mm and 2.0 mm DFT, FT and FP samples, showed VAF values lower than 85%. For each thickness, no significant differences were found between the two printing angles ($p > 0.05$), except for 2.0 mm thick samples from DFT, FT and GCT. In general, GCT showed the highest K values for all specimen thickness (Fig. 4).

The spectral behavior of the transmittance (Fig. 5) was similar for 0° and 90° groups, for all materials (VAF>98.0 %). Overall, the T % showed a significant increase from 2.0 to 0.5 mm thickness ($p < 0.001$) and good spectral behavior matches (VAF>98.5%) between thicknesses. Only 0.5 mm samples in comparison with 1.0, 1.5 and 2.0 mm samples for all the resins, showed VAF values lower than 75%. In general, GCT showed the lowest T % values for all specimen thickness (Fig. 5).

3D-printed samples presented albedo coefficient (a) values higher than 0.5 for all thicknesses and for 0° and 90° groups, except for wavelengths close to 400 nm (Fig. 6) in DFT and GCT. In general, a values are higher than 0.9 at 420 nm for all specimens; only 0.5 mm thickness specimens of FT and FP showed a values slightly below 0.9.

Light reflectivity (RI) values for all dental resins and both printing angles rapidly increased between 400 and 550 nm wavelengths (Fig. 7). The range of RI values were: 0.03–0.54 for DFT; 0.06–0.50 for FP; 0.04–0.51 for FT; and 0.03–0.65 for GCT. The RI values for 0.5 and 1.0 mm DFT samples and for 0.5 mm FT samples showed significant differences between both printing angles ($P < 0.01$). However, good spectral behavior matches (VAF>98.1 %) between thicknesses were found for all specimens.

The infinite optical thickness (X_∞) values for all 3D-printed resins, printing angles and thicknesses increased as the wavelength increased between 400 and 780 nm, with a similar spectral behavior (VAF>98.6%). Thus, the 3D-printed resins are opaquer at lower wavelengths than at high wavelengths (Fig. 8). The X_∞ values were found to be dependent on thickness, decreasing as the thickness increases ($p < 0.001$). For each thickness, no significant differences were found between the two printing angles ($p > 0.05$), except for 0.5 mm thick samples from all evaluated resins. The range of values for the experimental infinite optical thickness for the evaluated 3D-printed resins are presented in Table 3.

4. Discussion

Optical properties of 3D-printed dental resins can be mainly evaluated by the scattering (S) and absorption (K) coefficients, light reflectivity (RI) and infinite optical thickness (X_∞), and these parameters can be determined using two-flux Kubelka-Munk's (K-M) equations [19,20]. The two-flux models are very easy to implement since they are based on analytical formulas, allowing to deduce the K and S from measurements during the calibration step, and to make predictions once the model is calibrated. This is also very convenient when one uses a measuring device allowing only reflectance measurements.

The present study evaluated the effect of thickness and printing orientation on the spectral optical behavior of these biomaterials using two-flux K–M reflectance theory [21]. The results showed significant differences in optical properties values among the thicknesses evaluated for all materials used and both printing orientations. In addition, this study showed that as thickness of the 3D-printed resins increased, the absorption and scattering increased, and transmittance and infinite optical thickness decreased. These findings are in accordance with previous studies using dental resin-based composites [22–24,29,30]. Therefore, the first experimental hypothesis was accepted.

Overall, the T% and S-K coefficients values of the 3D-printed resins evaluated showed a similar spectral behavior. Thus, these materials

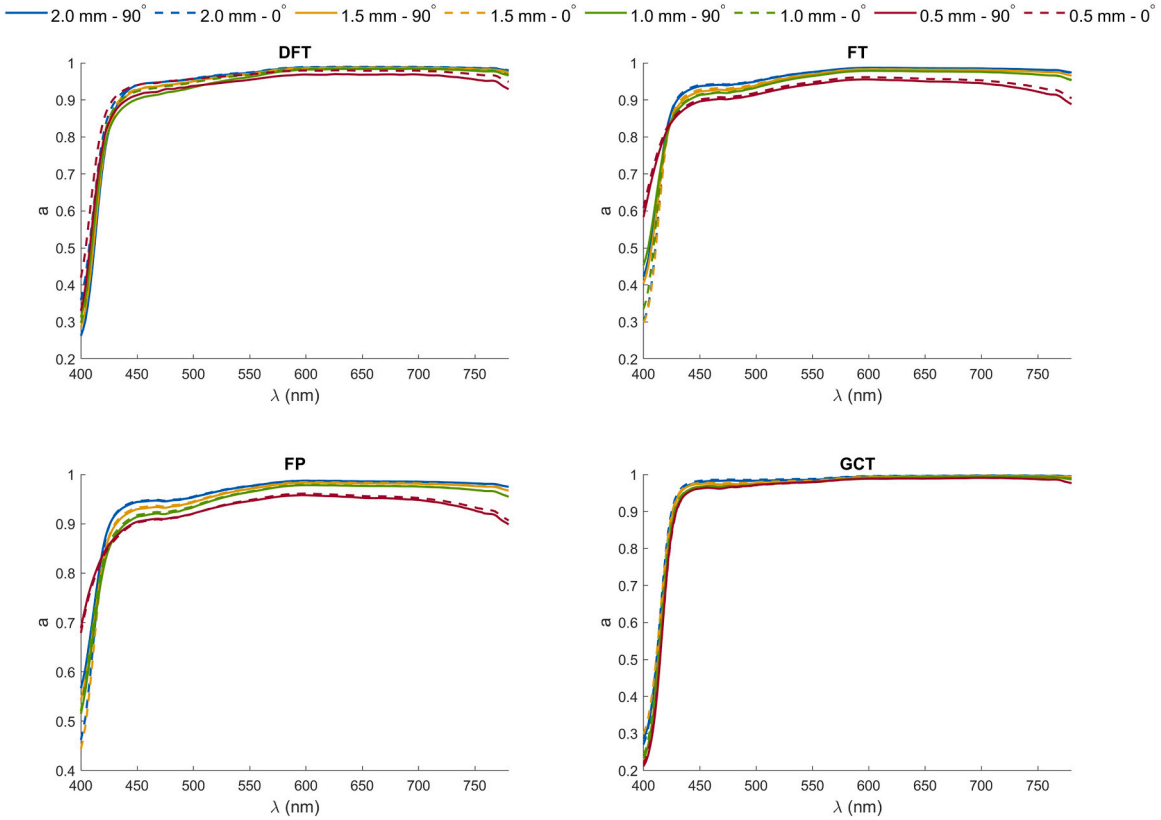

Fig. 6. Mean values of albedo coefficient (a) of all materials, thicknesses and printing orientation.

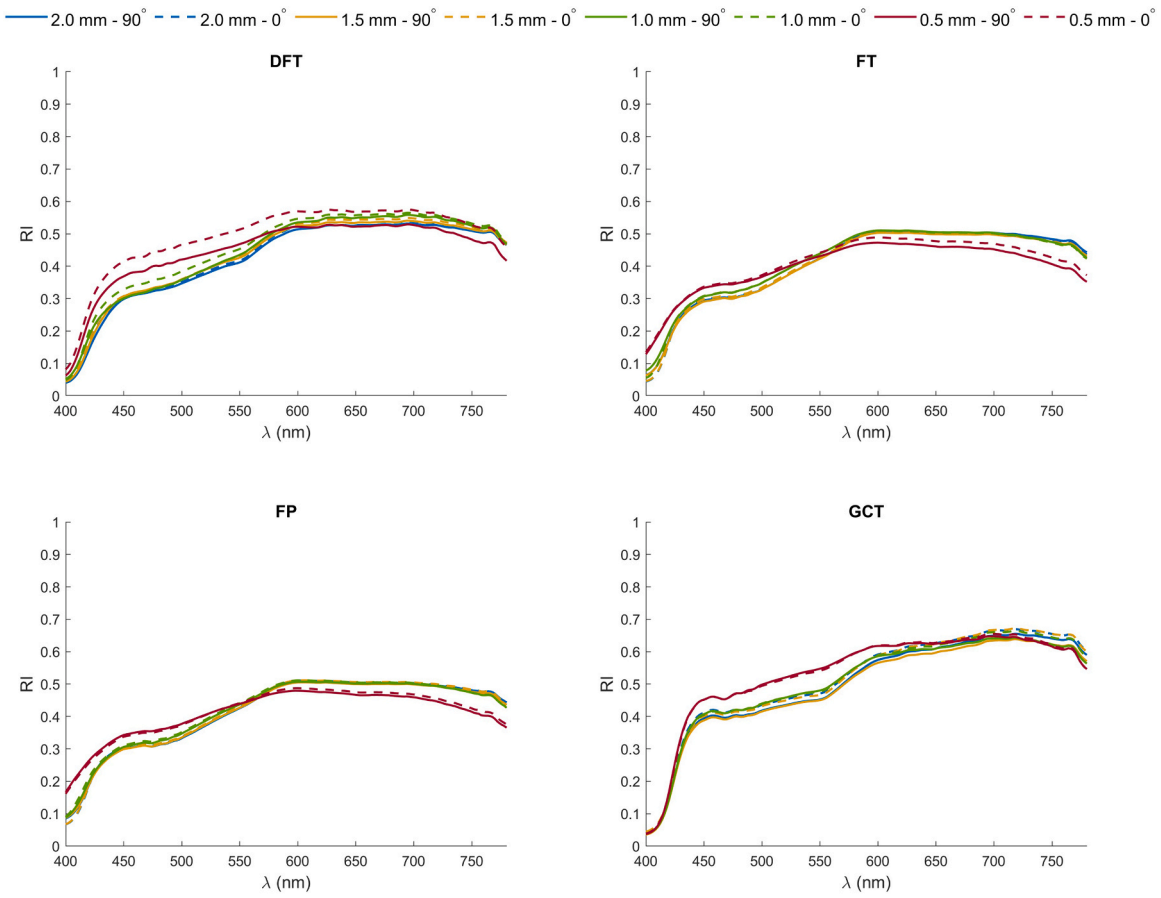

Fig. 7. Mean values of light reflectivity (RI) of all materials, thicknesses and printing orientation.

mainly scatter and absorb in short and medium wavelengths of visible light, and therefore, the maximum transmittance occurs for long wavelengths. The scattering coefficient of a resin-based composite is mainly determined by the particle size, and S reached largest when the particle diameter is equal to or larger than the wavelength of the incident light [22,31], while absorption is associated with the resin matrix and the nature of colorant pigments [32]. For each thickness evaluated, GCT showed significantly higher spectral scattering and absorption and lower transmittance than DFT, FT and FP materials (Figs. 3–5). This behavior may be because of differences in chemical composition, as GCT contains 20 wt % homogeneously dispersed silane-coated silica filler and anti-sedimentation fillers while DFT includes only a 0.8 wt % of silica filler content. The higher filler content could determine the higher scattering occurring in this material.

Albedo coefficient (a) values higher than 0.5 mean that scattering is the most relevant light attenuation phenomenon that occurs when light interacts with the material. In this study, except for wavelengths near 400 nm, the values of albedo (Fig. 6) are higher than 0.5 for all thicknesses and for both printing angles evaluated. In addition, these values are higher than 0.9 for medium and long wavelengths, which indicates the high prevalence of scattering on light transmittance for these dental resins, which could be also associated with the presence of a variable silica filler content and particle size. When light travels through a heterogenous medium, it can be scattered due to the anisotropy of the medium. When light finds an obstacle (particle) in the medium, a scattering event takes place, and the light-propagation direction changes; if light finds another obstacle, a new scattering event occurs and the light-propagation direction changes again. Thus, the scattering depends on the wavelength of irradiation, the refractive indexes of the medium, and the particle that causes the scattering, as well as on the particle size and its cross section [33,34].

The infinite optical thickness (X_∞) represents the thickness at which a translucent material, backed by a black background, will attain 99.9 % of its light reflectivity and become nearly opaque [35]. When the thickness of the restoration is thicker than the infinite optical thickness, the resin can exhibit its inherent color without being affected by the background color. Thus, the material thickness should exceed the infinite optical thickness of the same material so that the effect of background color can be eliminated. If such thickness could not be achieved, foundations on masking ability should be used to reduce or eliminate the influence from the background color.

The present study showed that 3D-printed resins are more opaque at lower wavelengths than at higher wavelengths (Fig. 8). For the visible wavelength range, all 0.5 mm and 1.0 mm thick 3D-printed specimens from both printing angles, were very thin compared to the infinite optical thickness. The thickness is similar to the infinite optical thickness only for the 1.5 mm specimens at wavelengths lower than 486 nm, and for the 2.0 mm specimens at wavelengths lower than 608 nm. Under these conditions, the background influences the reflected color of the 3D-printed resin for specimens thinner than 2.0 mm. However, these results differ from previous studies evaluating translucent resin composites at 1.0 mm thickness, with values between 10.4 and 12.6 mm [26]. Thus, the results of this study [26] suggest that the color of translucent resin composites may be more affected by the background than the 3D-printed resins.

Light reflectivity (RI) of resin composites describes their reflectance when are opaque and it can be used to obtain the intrinsic color of the composites independent of the background [36,37]. Thus, reflectivity can be described as the asymptotic reflectance as the thickness of the translucent material goes to infinity [19]. In this study, the absorption (K) and scattering (S) for each 3D-printed resin at different thicknesses (0.5, 1.0, 1.5 and 2 mm) and at 0° and 90°, were used to calculate RI

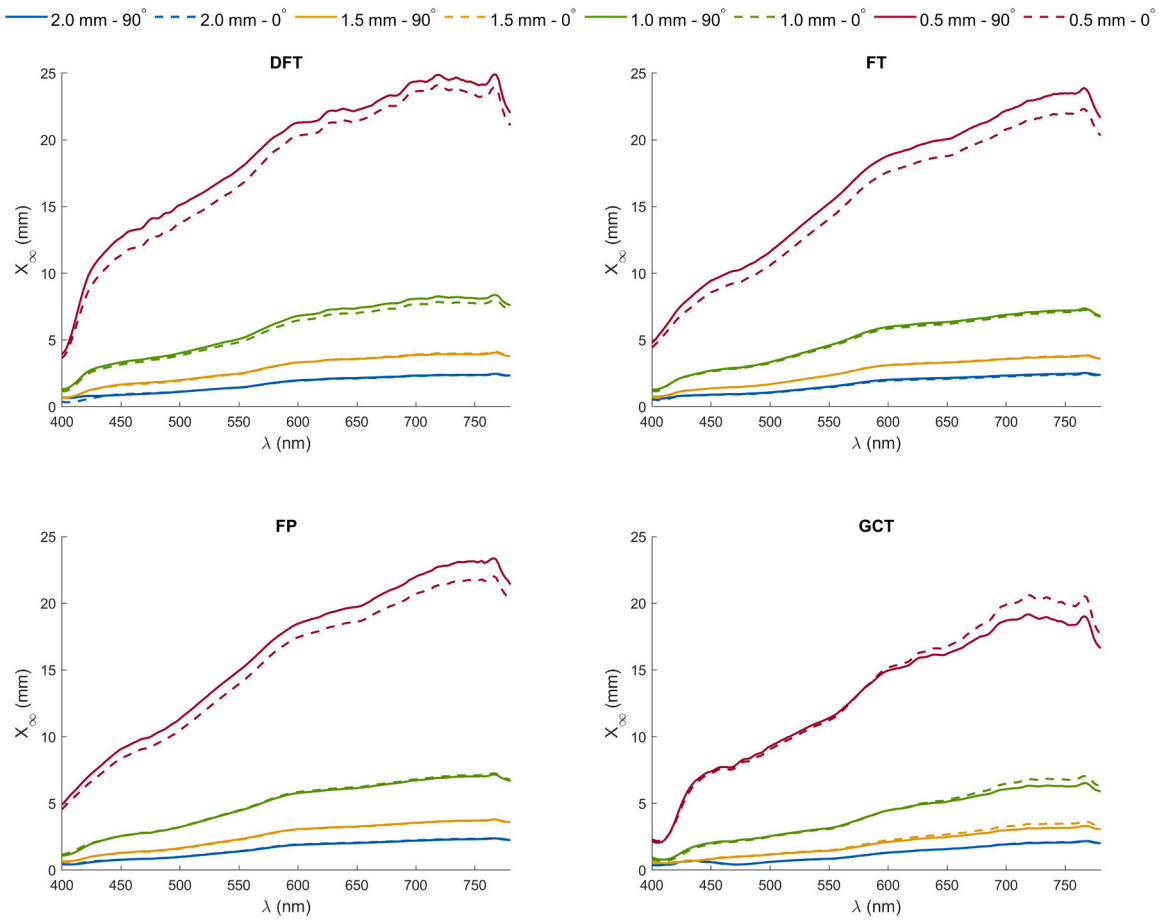

Fig. 8. Mean values of infinite optical thickness (X_∞) of all materials, thicknesses and printing orientation.

Table 3
Range of values for the experimental infinite optical thickness for the evaluated 3D-printed resins and both (0° and 90°) printing angles.

Materials	Thickness	X_∞ (0°) mm	X_∞ (90°) mm
DFT	0.5 mm	3.38–21.10	3.63–22.01
	1.0 mm	1.44–7.27	1.53–7.60
	1.5 mm	0.86–3.83	0.93–3.78
	2.0 mm	0.56–2.30	0.71–2.33
FP	0.5 mm	3.23–20.21	3.39–21.41
	1.0 mm	1.23–6.77	1.22–6.66
	1.5 mm	0.76–3.56	0.77–3.58
	2.0 mm	0.58–2.28	0.45–2.26
FT	0.5 mm	3.45–20.32	3.77–21.66
	1.0 mm	1.48–6.74	1.47–6.82
	1.5 mm	0.94–3.64	0.91–3.60
	2.0 mm	0.72–2.32	0.73–2.38
GCT	0.5 mm	2.82–20.53	2.83–19.02
	1.0 mm	1.25–6.27	1.28–5.90
	1.5 mm	0.81–3.32	0.90–3.07
	2.0 mm	0.54–2.05	0.46–2.02

[21]. The results showed that the reflectance at infinite thickness of the 3D-printed resins rapidly increased with the wavelength from 400 and 550 nm, and slightly decreased for long wavelengths (Fig. 7), regardless of the thickness.

A reflectivity spectrum may be used to predict the inherent CIELAB color parameters (L*, a*, b* or L*, C* and h°) of the 3D-printed resins for any CIE standard illuminant and CIE standard colorimetric observer. Further, the spectral reflectance at any clinically relevant thickness may be accurately predicted for any backing, based on the K–M optical coefficients, and therefore, the translucency parameter [38] for 3D-printed resins at any clinically relevant thickness may then be accomplished using these coefficients [21]. A recent study [39] evaluated the influence of printing orientation on color and translucency parameter of 3D-printed restorative resins using 1.0 mm thick specimens, showing that the building orientation (0° and 90°) influences the visual color and translucency and, therefore, the esthetic appearance of the resins. The results of the present study show significant differences in RI values at 0.5 and 1.0 mm between 0° and 90°, which could explain the effect of printing orientation on color and translucency. In addition, significant differences were found between both printing orientations for S and K, at 2.0 mm thickness; and in X_∞, at 0.5 and 1.0 mm for DFT, and at 0.5 mm for FT. Therefore, the second experimental hypothesis was accepted.

Future studies on clinically relevant thicknesses and building orientations based on light reflectivity should be performed to improve knowledge on adequate clinical application of 3D-printed dental restorative resins. Such rationale should assist manufacturers on producing new 3D printing resins.

Therefore, the biomimetic of 3D-printed resins is ruled by the interaction of three different components: the color of the backing, its thickness, and the material basic optical properties. Since Kubelka-Munk reflectance theory can be used as an accurate simplified model for translucent materials [21], it can be applied to calculate both the scattering and absorption coefficients for 3D-printed dental resins and other optical properties (T%, RI and XI). To enhance materials development and better understand the optical properties of 3D-printed materials in restorative dentistry, in vitro studies are required, such as the presented work. Thus, by studying how different factors (thickness and build orientation) affect these materials, their behavior and predictability for clinical use can be improved.

5. Conclusions

Understanding the optical behavior of 3D-printed restorative dental resins is crucial to optimize their clinical effectiveness. Although the 3D printing resin systems evaluated showed similar spectral optical behavior the values of S, K, T% and X_∞ significantly vary between thicknesses. Scattering is the most relevant light attenuation phenomenon in 3D-printed resins. The choice of the building orientation (0° or 90°) could affect the optical properties of the 3D-printed resins. Therefore, structural thickness and building orientation should be considered in order to improve the biomimetic capacity of 3D-printed dental restorative resins.

Data Availability

The data that support the findings of this study are included in it. The documents are available on request from the corresponding author.

Acknowledgements

The authors acknowledge funding support from the FEDER/ Government of Andalusia P20-00200 and State of Rio Grande do Sul, FAPERGS (grant #19/2551-0001721-9). Funding for open access charge: Universidad de Granada / CBUA.

The authors also acknowledge Detax GmbH, Formlabs Inc. and GC Corporation for providing the polymer-based 3D printing restorative resins used in this study.

References

[1] Kessler A, Hickel R, Reymus M. 3D printing in dentistry-state of the art. Oper Dent 2020;45:30–40. https://doi.org/10.2341/18-229-L.
[2] Stansbury JW, Idacavage MJ. 3D printing with polymers: challenges among expanding options and opportunities. Dent Mater 2016;32(1):54–64. https://doi.org/10.1016/j.dental.2015.09.018.
[3] Della Bona A, Cantelli V, Britto VT, Collares FK, Stansbury JW. 3D printing restorative materials using a stereolithographic technique: a systematic review. Dent Mater 2021;37(2):336–50. https://doi.org/10.1016/j.dental.2020.11.030.
[4] Wadei MHD, Gupta SG, Othman AA, Alshehri AH, Alqarni H, Mobarki AH, et al. Physical and mechanical properties of 3D-printed provisional crowns and fixed dental prosthesis resins compared to CAD/CAM milled and conventional provisional resins: a systematic review and meta-analysis. Polymers 2022;14(13):2691. https://doi.org/10.3390/polym14132691.
[5] Soto- Montero J, de Castro EF, Romano BC, Nima G, Shimokawa CAK, Giannini M. Color alterations, flexural strength and microhardness of 3D printed resins for fixed provisional restoration using different post-curing. Dent Mater 2022;38:1271–82. https://doi.org/10.1016/j.dental.2022.06.023.
[6] Kim D, Shim JS, Lee D, Shin SH, Nam NE, Park KH, et al. Effects of post-curing time on the mechanical and color properties of three-dimensional printed crown and bridge materials. Polymers 2020;12(11):2762. https://doi.org/10.3390/polym12112762times.
[7] Reymus M, Fabritius R, Keßler A, Hickel R, Edelhoff D, Stawarczyk B. Fracture load of 3D-printed fixed dental prostheses compared with milled and conventionally fabricated ones: the impact of resin material, build direction, post-curing, and artificial aging-an in vitro study. Clin Oral Invest 2020;24(2):701–10. https://doi.org/10.1007/s00784-019-02952-7.
[8] Alharbi N, Osman RB, Wismeijer D. Factors influencing the dimensional accuracy of 3D-printed full-coverage dental restorations using stereolithography technology. Int J Prosthodont 2016;29(5):503–10. https://doi.org/10.11607/ijp.4835.
[9] Keßler A, Hickel R, Ilie N. In vitro investigation of the influence of printing direction on the flexural strength, flexural modulus and fractographic analysis of 3D-printed temporary materials. Dent Mater J 2021;40(3):641–9. https://doi.org/10.4012/dmj.2020-147.
[10] Alharbi N, Osman R, Wismeijer D. Effects of build direction on the mechanical properties of 3D-printed complete coverage interim dental restorations. J Prosthet Dent 2016;115(6):760–7. https://doi.org/10.1016/j.prosdent.2015.12.002.
[11] Unkovskiy A, Bui PH, Schille C, Geis-Gerstorfer J, Huettig F, Spintzyk S. Objects build orientation, positioning, and curing influence dimensional accuracy and flexural properties of stereolithographically printed resin. Dent Mater 2018;34(12):e324–33. https://doi.org/10.1016/j.dental.2018.09.011.
[12] Shim JS, Kim JE, Jeong SH, Choi YJ, Ryu JJ. Printing accuracy, mechanical properties, surface characteristics, and microbial adhesion of 3D-printed resins with various printing orientations. J Prosthet Dent 2020;124(4):468–75. https://doi.org/10.1016/j.prosdent.2019.05.034.
[13] Derban P, Negrea R, Rominu M, Marsavina L. Influence of the printing angle and load direction on flexure strength in 3D printed materials for provisional dental restorations. Materials 2021;14(12):3376. https://doi.org/10.3390/ma1412337.
[14] Espinar C, Della Bona A, Pérez MM, Pulgar R. Color and optical properties of 3D printing restorative polymer-based materials: a scoping review. J Esthet Restor Dent 2022;34(6):853–64. https://doi.org/10.1111/jerd.12904.
[15] Tian Y, Chen C, Xu X, Wang J, Hou X, Li K, et al. A review of 3D printing in dentistry: technologies, affecting factors and applications. Scanning 2021;(9950131):1–19. https://doi.org/10.1155/2021/9950131.
[16] Tahayeri A, Morgan M, Fugolin AP, Bompolaki D, Athirasala A, Pfeifer CS, et al. 3D printed versus conventionally cured provisional crown and bridge dental materials. Dent Mater 2018;34(2):192–200. https://doi.org/10.1016/j.dental.2017.10.003.
[17] Wang LV, Wu HI. Biomedical optics. Principles and imaging. United States: John Wiley & Sons Inc.-Interscience; 2007.
[18] Dunsby C, French PMW. Techniques for depth-resolved imaging through turbid media including coherence-gated imaging. J Phys D: Appl Phys 2003;36(14):207–27. https://doi.org/10.1088/0022-3727/36/14/201.
[19] Kubelka P. New contributions to the optics of intensely light-scattering materials. J Opt Soc Am 1948;38:448–57. https://doi.org/10.1364/JOSA.38.000448.
[20] Kubelka P. New contributions to the optics of intensely light-scattering materials. Part II: nonhomogeneous layers. J Opt Soc Am 1954;44:330–5. https://doi.org/10.1364/JOSA.44.000330.
[21] Mikhail SS, Sazer SS, Johnston WM. Accuracy of Kubelka Munk reflectance theory for dental resin composite material. Dent Mater 2012;(28):729–35. https://doi.org/10.1016/j.dental. 2012.03.006.
[22] Lucena C, Ruiz-Lopez J, Pulgar R, Della Bona A, Pérez MM. Optical behavior of one-shaded resin-based composites. Dent Mater 2021;37:840–8. https://doi.org/10.1016/j.dental.2021.02.011.
[23] Pérez MM, Hita-Iglesias C, Ghinea R, Yebra A, Pecho OE, Ionescu AM, et al. Optical properties of supra-nano spherical filled resin composites compared to nanofilled, nano-hybrid and micro-hybrid composites. Dent Mater J 2016;35(3):353–9. https://doi.org/10.4012/dmj.2015-126.
[24] Pecho OE, Ghinea R, Navarro do Amaral EA, Cardona JC, Della Bona A, Pérez MM. Relevant optical properties for direct restorative materials. Dent Mater 2016;32(5):e105–12. https://doi.org/10.1016/j.dental.2016.02.008.
[25] Gouveia D, Yilmaz B, Cevik P, Johnston WM. Using Kubelka-Munk reflectance theory to predict optimal pink composite thickness and shade with an opaqued PEEK background for a final gingival color: An in vitro study. Dent Mat 2022;38:1452–8. https://doi.org/10.1016/j.dental.2022.06.027.
[26] Li R, Ma X, Liang S, Sa Y, Jiang T, Wang Y. Optical properties of enamel and translucent composites by diffuse reflectance measurements. J Dent 2012;40:e40–7. https://doi.org/10.1016/j.jdent.2012.04.016.
[27] Molenaar R, ten Bosch JJ, Zijp JR. Determination of Kubelka–Munk scattering and absorption coefficients by diffuse illumination. Appl Opt 1999;38(10):2068–77. https://doi.org/10.1364/AO.38.002068.
[28] Roy A, Ramasubramaniam R, Gaonkar HA. Empirical relationship between Kubelka-Munk and radiative transfer coefficients for extracting optical parameters of tissues in diffusive and nondiffusive regimes. J Biomed Opt 2012;17(11):115006. https://doi.org/10.1117/1.JBO.17.11.115006.
[29] Lucena C, Benavides-Reyes C, Ruiz-Lopez J, Tejada-Casado M, Pulgar R, Pérez MM. Relevant optical properties for gingiva-colored resin-based composites. J Dent 2022;126:104316. https://doi.org/10.1016/j.jdent.2022.104316.
[30] Arimoto A, Nakajima M, Hosaka K, Nishimura K, Ikeda M, Foxton RM, et al. Translucency, opalescence and light transmission characteristics of light-cured resin composites. Dent Mater 2010;26:1090–7. https://doi.org/10.1016/j.dental.2010.07.009.
[31] Lee Y. Influence of scattering/absorption characteristics on the color of resin composites. Dent Mater 2007;23:124–31. https://doi.org/10.1016/j.dental.2006.01.007.
[32] Arikawa H, Kanie T, Fujii K, Takahashi H, Ban S. Effect of filler properties in composite resins on light transmittance characteristics and color. Dent Mater J 2007;26:38–44. https://doi.org/10.4012/dmj.26.38.
[33] Fernández-Oliveras A, Rubiño M, Pérez MM. Scattering anisotropy measurements in dental tissues and biomaterials. J Eur Opt Soc Rap Public 2012;7:12016. https://doi.org/10.2971/jeos.2012.12016.
[34] Grajower R, Wozniak WT, Lindsay JM. Optical properties of composite resins. J Oral Rehabil 1982;9:389–99. https://doi.org/10.1111/j.1365-2842.1982.tb01027.x.
[35] Yeh CL, Miyagawa Y, Powers JM. Optical properties of composites of selected shades. J Dent Res 1982;61:797–801. https://doi.org/10.1177/00220345820610062901.
[36] Powers JM, Yeh CL, Miyagawa Y. Optical properties of composites of selected shades in white light. J Oral Rehabil 1983;10:319–24. https://doi.org/10.1111/j.1365-2842.1983.tb00126.x.
[37] Yeh CL. The color and optical properties of shaded composites. Master's Thesis. Ann Arbor, MI: University of Michigan; 1981. p. 104.
[38] Johnston WM, Ma T, Kienle BH. Translucency parameter of colorants for maxillofacial prostheses. Int J Prosthodont 1995;8(1):79–86. https://doi.org/10.5958/2394-2800.2016.00014.6.
[39] Espinar C, Della Bona A, Pérez MM, Tejada-Casado M, Pulgar R. The influence of printing angle on color and translucency of 3D printed resins for dental restorations. Dent Mater 2023;39:410–7. https://doi.org/10.1016/j.dental.2023.03.011.